iScience

CellPress
OPEN ACCESS

Article

Exploiting elastic buckling of high-strength gold nanowire toward stable electrical probing

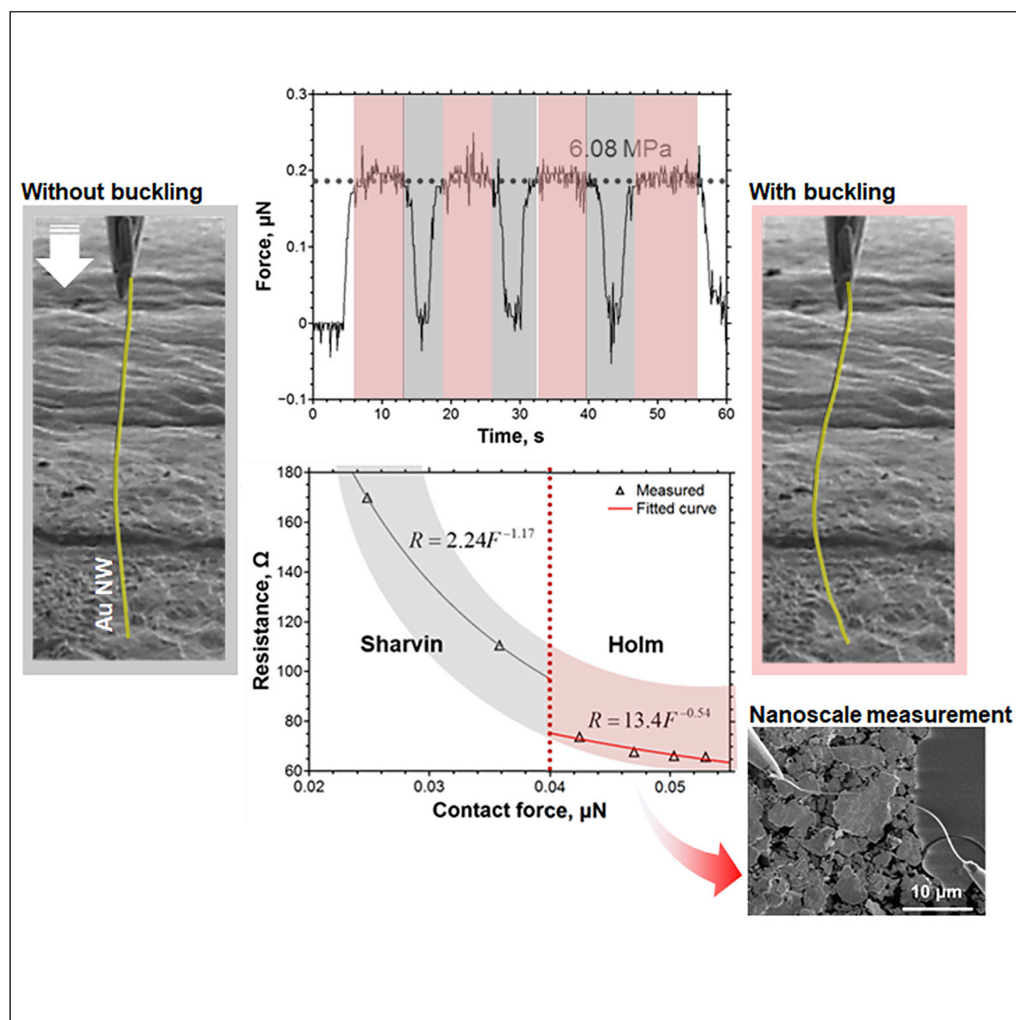

Jong-Hyun Seo, Sung-Gyu Kang, Yigil Cho, ..., Bongsoo Kim, In-Suk Choi, Jae-Pyoung Ahn

insukchoi@snu.ac.kr (B.K.)
bongsoo@kaist.ac.kr (I.-S.C.)
jpahn@kist.re.kr (J.-P.A.)

Highlights

A defect-free single crystalline Au nanowire shows the Euler buckling deformation

The buckling and post-buckling deformation is utilized for the electrical measurement

Contact regime changes from the Sharvin to the Holm during buckling deformation

This study suggests a nanoscale probe for the electrical and magnetic characterization

Seo et al., iScience *25*, 105199
October 21, 2022 © 2022 The Authors.
https://doi.org/10.1016/j.isci.2022.105199

Check for updates

iScience

CellPress
OPEN ACCESS

Article

Exploiting elastic buckling of high-strength gold nanowire toward stable electrical probing

Jong-Hyun Seo,[1,6] Sung-Gyu Kang,[2,6] Yigil Cho,[2] Harold S. Park,[3] Youngdong Yoo,[4,5] Bongsoo Kim,[4,*] In-Suk Choi,[2,7,*] and Jae-Pyoung Ahn[1,*]

SUMMARY

Buckling is a loss of structural stability. It occurs in long slender structures or thin plate structures which is subjected to compressive forces. For the structural materials, such a sudden change in shape has been considered to be avoided. In this study, we utilize the Au nanowire's buckling instability for the electrical measurement. We confirmed that the high-strength single crystalline Au nanowire with an aspect ratio of 150 and 230-nm-diameter shows classical Euler buckling under constant compressive force without failure. The buckling instability enables stable contact between the Au nanowire and the substrate without any damage. Clearly, the *in situ* electrical measurement shows a transition of the contact resistance between the nanowire and the substrate from the Sharvin (ballistic limit) mode to the Holm (Ohmic) mode during deformation, enabling reliable electrical measurements. This study suggests Au nanowire probes exhibiting structural instability to ensure stable and precise electrical measurements at the nanoscale.

INTRODUCTION

Buckling instability is an abrupt change in the geometry of a material subjected to an external force. It leads to a considerable out-of-plane deflection in the slender features such as beam and plate. Hence, for the structural materials, buckling instability has been considered to be avoided and prevented. In small-scale materials, this sudden deformation becomes more important. For the nanowires and thin films which have become essential components in advanced electronics, their buckling deformation causes imminent failure of device, which compromises the mechanical reliability (Hsin et al., 2008; Ji et al., 2007; Kleinbichler et al., 2018; Song et al., 2008a, 2008b; Wang and Feng, 2009).

Recently, researchers have shown that buckling instability is advantageous in new engineering applications. The large buckling and post-buckling deformation occurring under constant stress enable the nanomaterials showing buckling instability to be utilized as sensors (Begley and Barker, 2007; Dobrokhotov et al., 2008; Elvin et al., 2006; Kiyono et al., 2012), isolator (Avramov and Mikhlin, 2016; Shaw et al., 2013), and energy absorber (Cottone et al., 2012; Ramlan et al., 2012; Van Blarigan et al., 2012; Yang et al., 2009; Zhu and Zu, 2013). Moreover, owing to the completely reversible buckling deformation, researchers have proposed pre-buckled nanomaterials for stretchable electronics (Sun et al., 2006; Zhou et al., 2019) and microelectromechanical systems (Erbil et al., 2020). In this respect, the characteristics of buckling instability combined with the intrinsic properties of nanomaterials may open new possibilities for future innovative applications.

A nanoscale electrical measurement has been the subject of intense theoretical and experimental research as it may provide electron transport information at the nanoscale level. However, probing electrical transport on the nanoscale is inherently difficult because of solid contact problems such as nonlinear mechanical and electrical effects. When the conventional probe, such as the tungsten (W) probe, directly contacts the subject under a high contact force, the probe can be blunted or the sample surface can be damaged easily. On the other hand, if the contact force is too low, the contact area between the sample and the probe becomes too small. It leads to a significant increase in the contact resistance and non-linear electrical effects, which makes it very difficult to accurately measure the resistance of the sample.

Here, we use the high-strength single crystalline gold nanowires (Au NWs) exhibiting buckling instability to demonstrate stable contact electrical probing without damaging the sample. We took advantage of the mechanical instability of the Au NW, namely the Euler buckling, which has been recognized as a vulnerable, thus

[1]Advanced Analysis Center, Korea Institute of Science and Technology, Seoul 02792, Korea

[2]Department of Materials Science and Engineering, Seoul National University, Seoul 08826, Korea

[3]Department of Mechanical Engineering, Boston University, Boston, MA 02215, USA

[4]Department of Chemistry, Korea Advanced Institute of Science and Technology, Daejeon 34141, Korea

[5]Department of Chemistry, Ajou University, Suwon 16499, Korea

[6]These authors contributed equally

[7]Lead contact

*Correspondence: insukchoi@snu.ac.kr (B.K.), bongsoo@kaist.ac.kr (I.-S.C.), jpahn@kist.re.kr (J.-P.A.)

https://doi.org/10.1016/j.isci.2022.105199

This is an open access article under the CC BY-NC-ND license (http://creativecommons.org/licenses/by-nc-nd/4.0/).

undesirable deformation. Paradoxically, the buckling of the nanowire probe leads to a very stable electrical contact, which results in quite low and constant contact resistance. Through *in situ* monitoring of the electrical transport during the electrical contact between the nanowire probe tip and the metal electrode, we found that the transport regime changed from quantum ballistic transport to classical diffusive transport. Furthermore, to reliably measure electrical resistance without having to worry about variation in the contact force of the probe. By using this feature, we could measure the resistance of a small-scale area without damaging the sample. Hence, our accurate electrical measurement by direct contact provides a robust solution for nano-scale electrical measurement and furthermore will open the new possibility of scanning probe microscope.

RESULTS AND DISCUSSION

Euler buckling of Au nanowire

A single-crystalline Au nanowire (NW) in this study exhibits classical Euler buckling when subjected to compressive loadings. We used defect-free [110] Au NWs with a rhombic cross-section bounded by four surfaces (Hwang et al., 2015). The defect-free Au NWs were fabricated via a vapor transport method where direction, diameter, and length can be precisely controlled by adjusting the atom flux and the reaction time (Kang et al., 2015; Yoo et al., 2010). Figure 1A and Video S1 show a vertically standing Au NW with a diameter of 230 nm and length of 35 μm continuously deformed by the tungsten tip moving along the axial direction of NW. This both-ends-pinned NW exhibits large lateral deflection when the tip moves downward and subsequently recovers its straight shape when the tip moves upward. Apparently, this deflection is the same as the buckled shape of a classical beam that has both ends pinned, as shown in Figure 1B. For more quantitative measurement, we conducted the *in situ* compression test of Au NWs by fixing one end of the NW to a tungsten tip with nanomanipulator (MM3A, Kleindeck) and the other end to a silicon cantilever of the force measurement system (FMS, Kleindeck) (Seo et al., 2011). Figure 1C and Video S2 show a serial snapshot of NW (diameter of 230 nm and length of 35 μm) during deformation and Figure 1D shows the corresponding force response as a function of time. During the uniaxial compression, the Au NW shows a clear stepwise deformation. The compression load rapidly increased from 0 to 0.33 μN at about 6 s, and then the load remained constant. Moreover, the buckling load remained constant even during partial unloading and reloading between 32 and 65 s, which reflects ideal buckling stability. From the Euler buckling theory, the critical buckling load could be calculated as follows: (Timoshenko and Gere, 1961)

$$F_{cr} = \frac{\pi^2 EI}{(KL)^2} \quad \text{(Equation 1)}$$

where F_{cr} is the critical buckling load, E is Young's modulus of the NW (81 GPa for an Au nanowire oriented in the [110] direction) (Seo et al., 2011), I is the area moment of inertia, L is the length of the NW, and K is a dimensionless coefficient known as the effective-length factor (0.5 for a wire fixed at both ends). Equation 1 gives the critical buckling load of 0.36 μN close to the experimentally obtained value (0.33 μN), suggesting that the Au NW in this study exhibits the classical Euler buckling behavior when subjected to the compressive loading. Figure 1E shows the von Mises stress distribution inside the buckled NW calculated by the finite element (FE) model. The highest stress of 700 MPa is developed at the surface of the NW. It was reported that, owing to the defect-free microstructure, the [110] Au NW exhibits a high yield strength of 1 GPa (Seo et al., 2011). Furthermore, the defect-free Au nanowire is beneficial for fatigue resistance, as the pre-existing dislocations under cyclic loadings within elastic limits lead to the formation of intrusions and extrusions which act as a stress concentration point for crack initiation. Accordingly, it can be deduced that the buckling and the post-buckling deformations of Au NW in this study are reversible. Consistently, a force response from another cyclic buckling experiment in Figure 1F (NW's diameter of 200 nm and length of 40 μm) shows that the stepwise response is almost the same even under multiple loading and unloading. In this case, the Au NW exhibits buckling deformation at lower compression load (0.2 μN) compared to the Au NW in Figure 1D. It is attributed to the different cross-sectional areas of the Au NW. Equation 1 gives the critical buckling load of 0.19 μN for the Au NW with a diameter of 200 nm and length of 35 μm. Therefore, these results clearly demonstrate that the defect-free single-crystalline [110] Au NWs are highly flexible and exhibit reversible Euler buckling behavior when subjected to uniaxial compressive load.

Contact resistance change by Euler buckling of Au nanowire

We now demonstrate that the Euler buckling of Au NW enables a low and stable electrical contact resistance while minimizing sample damage during electrical contact probing. First, we measured the electrical contact resistance between a bulk Au electrode and the Au NW (Figure 2). After the Au electrode and the

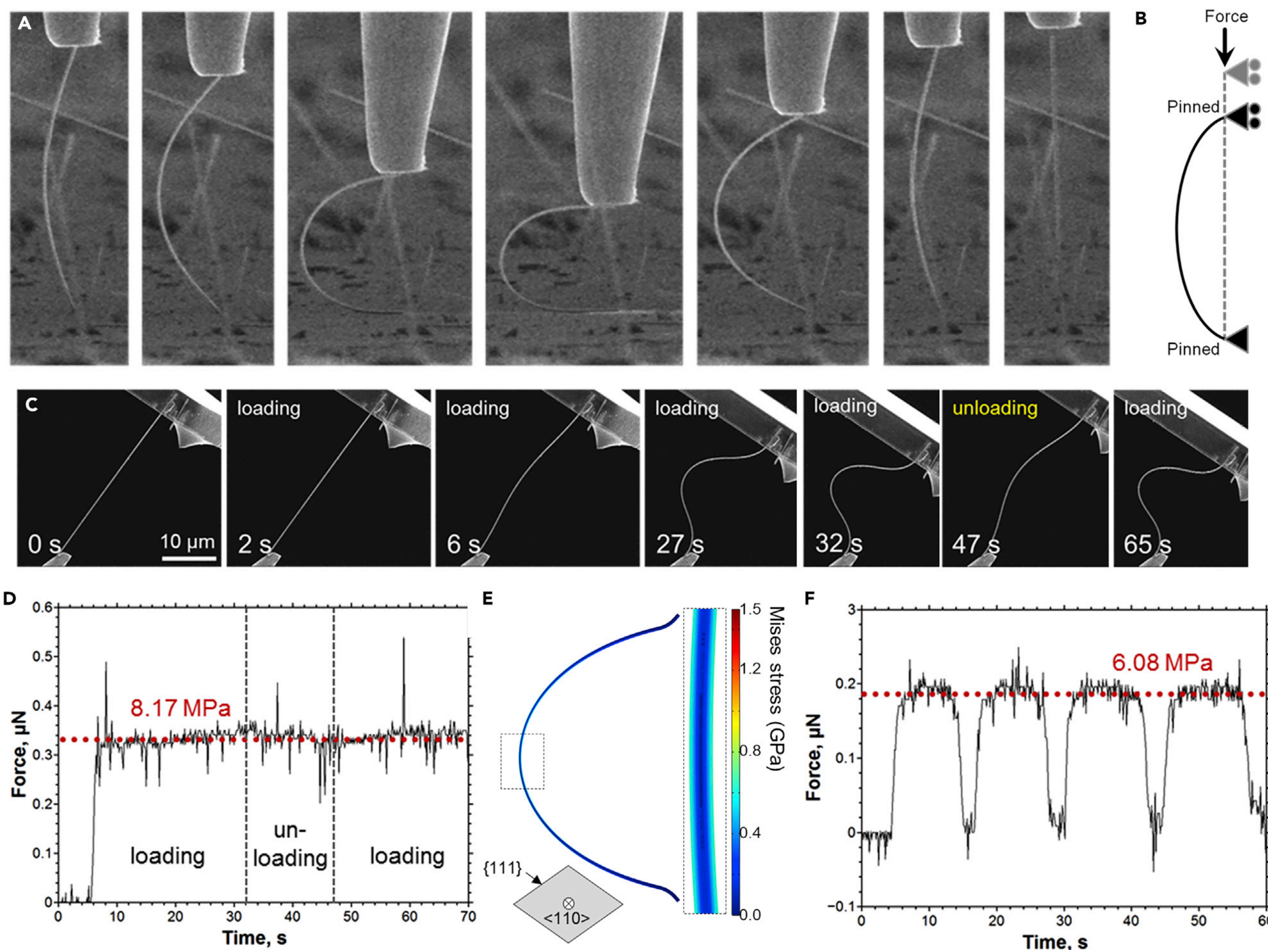

Figure 1. Euler buckling of single-crystalline Au nanowire

(A) Snapshots on the deformation of a both-ends-pinned Au nanowire.

(B) Buckled shape of the classical both-ends-pinned beam.

(C and D) Snapshots on the deformation of a both-ends-fixed Au nanowire and corresponding force-time plot during the deformation (diameter of 230 nm and length of 35 μm).

(E) Stress distribution inside the Au nanowire during the deformation.

(F) Force-time plot during the deformation of a both-ends-fixed Au nanowire under complete loading and unloading (diameter of 200 nm and length of 35 μm).

Au NW with one end fixed to the tungsten tip (Figure S1) were brought into contact, the current-voltage (I-V) curves of the system were measured at various vertical displacements of fixed end of NW (0 to 700 nm) inducing the Euler buckling (Figure 2A). Notably, the contact between the Au NW and the electrode allows a rotation of NW around the contact point analogous to the pinned end, making the contact area increases with the buckling deflection. Expectedly, as shown in Figures 2A and 2B, the buckling deformation of NW is the same as the buckled shape of the fixed-pinned beam.

The more buckled the Au NW is, the lower the contact resistance is. Figure 2C shows the I-V curves of the system at various vertical displacements. Commonly, the I-V curves are linear, but there are changes in the slope, i.e., the total resistance of system, at I = 0.55 and 0.65 mA in the NWs buckled by the vertical displacements of 100 and 200 nm, respectively. This resistance change is attributed to the small quantum-transport contacts, which will be discussed later. Excluding the resistance change by the small quantum-transport contacts, the total resistance decreases with the vertical displacement of NW. The averaged total resistance as a function of the vertical displacement of NW in Figure 2D shows a clear trend. The total resistance decreases from 32.9 kΩ and finally approaches 60 Ω at a vertical displacement of about 300 nm. The measured resistance consists of the contact resistance and the intrinsic resistance of the Au nanowire,

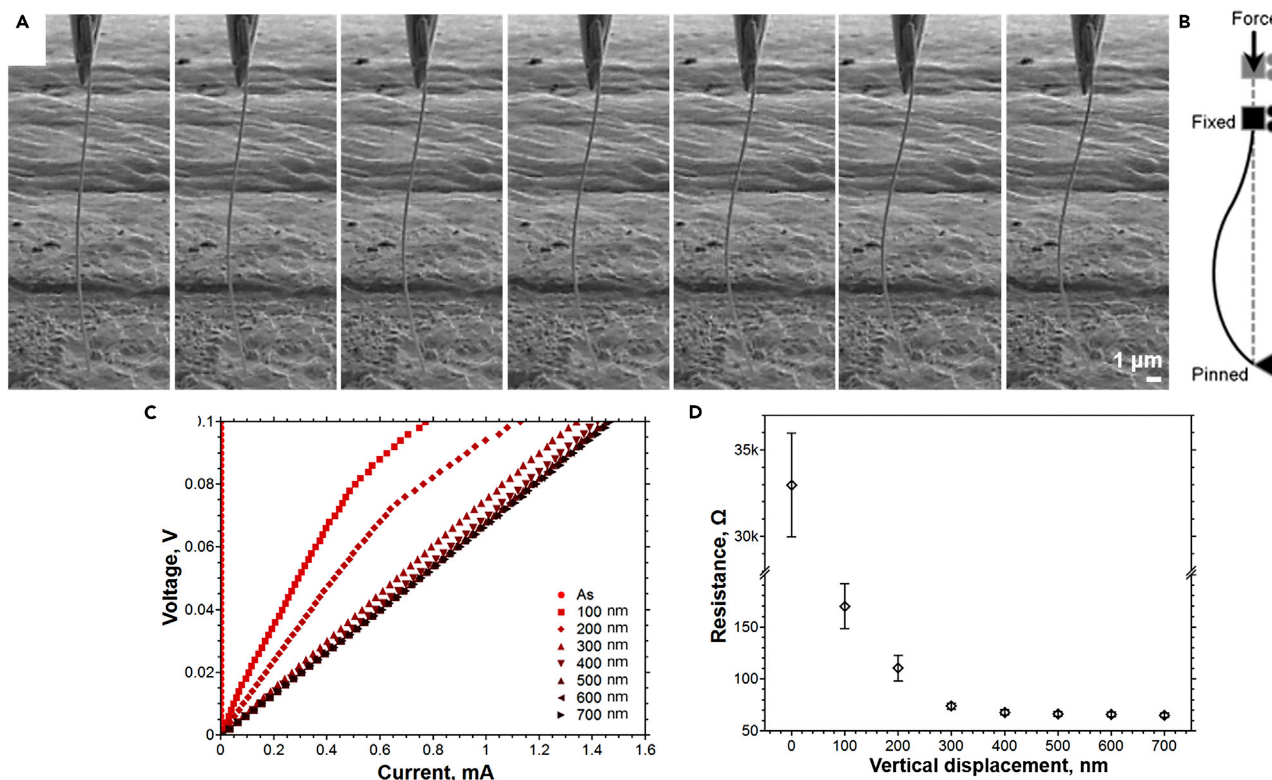

Figure 2. Contact resistance of single-crystalline Au nanowire during Euler buckling deformation

(A) Snapshots on the deformation of a fixed-pinned Au nanowire during electrical measurement.

(B) Buckled shape of the classical fixed-pinned beam.

(C) I-V curves in the nanowire measured at various vertical displacements inducing Euler buckling of nanowire.

(D) Resistance of system at various vertical displacements.

which depends on the diameter and length of the nanowire. Thus, the contact resistance can be isolated by subtracting the intrinsic resistance of the Au nanowire from the total resistance. The intrinsic resistance in the Au nanowire was about 24.08 Ω, which was measured using a nanoscale four-point-probe method directly contacting nanoprobes at an Au nanowire (Figure S2). The change in resistance in Figure 2D, therefore, is attributed to the decrease in the contact resistance.

The decrease in contact resistance reflects the nanoscale-specific nature of contact resistance. Specifically, metal-to-metal contact poses numerous restrictions against electrical conduction because of the nanoscale roughness of the contact interface. At a nanoscale contact, two types of contact resistance can arise depending on the contact radius of the probe tip: Sharvin contact resistance which is associated with ballistic electron transport, and Holm contact resistance which is associated with diffusive electron transport. The Sharvin contact resistance ($R_{sharvin}$) is analytically given as (Sharvin, 1965),

$$R_{sharvin} = \frac{4\rho\lambda}{3\pi a^2} \quad \text{(Equation 2)}$$

where ρ is the resistivity, λ is the electron mean free path, and a is the contact radius. The Holm contact resistance (R_{Holm}), on the other hand, is derived based on the classical Maxwell equation as (Holm, 1967),

$$R_{Holm} = \frac{\rho}{2a} \quad \text{(Equation 3)}$$

In both regimes, the resistance decreases with increasing contact area. However, the contact radius between the probe tip and the surface is the main criterion for transitioning from Sharvin to Holm contact resistance. The Sharvin contact resistance occurs at the diffusive limit of electron transport where the contact radius is considerably smaller than the electron mean free path. However, if the probe tip is pressed against the electrode surface so that the contact radius becomes larger than the electron mean free

CellPress
OPEN ACCESS

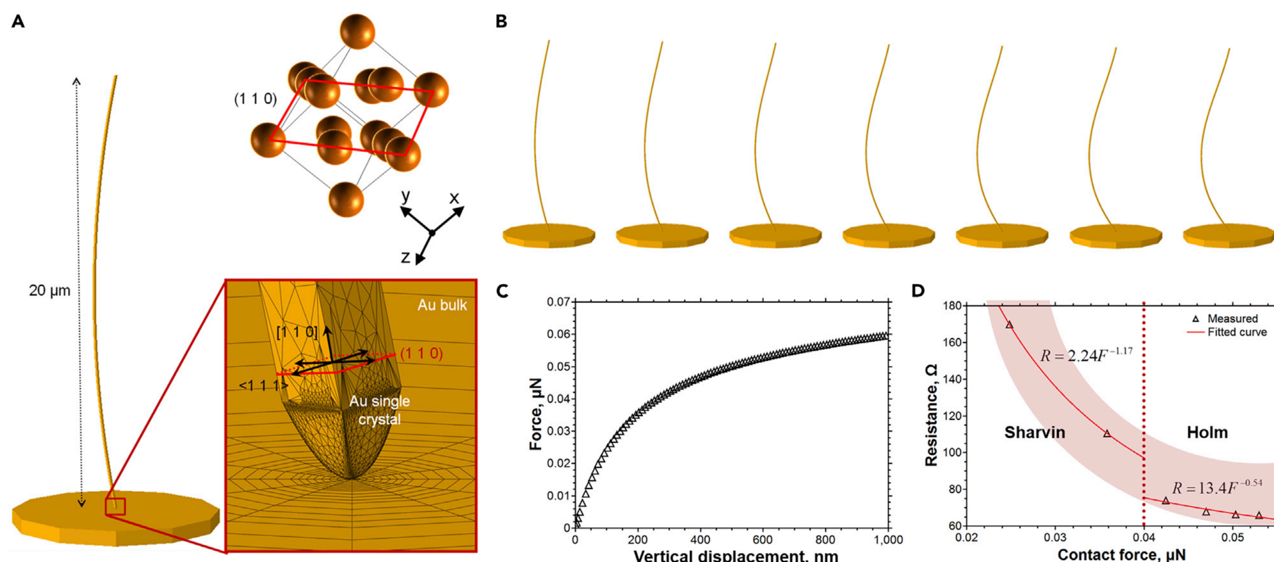

Figure 3. Change in contact resistance of single-crystalline Au nanowire induced by contact area change during Euler buckling deformation

(A) Finite element mesh and crystallographic orientation of Au nanowire.

(B) Simulation of ideal buckling behavior of an Au nanowire that contacts a bulk Au electrode.

(C) Calculated relation between the contact force and the down displacement.

(D) A relation between the contact resistance and the contact force of single-crystalline Au nanowire.

path of the medium, the electron transport through the contact should be treated as a classical Holm contact. Quantitative analysis of the change in resistance enabled us to assess the electron transport regime during buckling. The contact radius is a function of contact force at the probe tip according to classical contact mechanics. Hence, without loss of generality, Equations 2 and 3 can be combined into Equation 4 to give the relation between the contact resistance (R) and the contact force (F_c), which is the compressive force applied to the nanowires (Mikrajuddin et al., 1999; Vandamme, 1974).

$$R = f(F_c) \propto \frac{1}{F_c^{\,n}} \quad \text{(Equation 4)}$$

In particular, the exponent of the relation is a fingerprint for differentiating between the Holm and Sharvin contact resistances. The exponent becomes 1/3 for Holm resistance and 2/3 for Sharvin resistance for an elastically deformed spherical contact. On the other hand, the exponent is 1/2 for Holm resistance and 1 for Sharvin resistance for a plastically deformed spherical contact. We applied the above criteria, assuming that our nanowire probe tip was spherical.

As our experimental system could not be used to simultaneously perform force and electrical measurements, we need to establish the relationship between the vertical displacement of NW and the corresponding contact force, which is equivalent to the compressive force applied to the nanowire. To do so, we constructed the FE model based on the actual geometry of Au NW (Figure 3A). In the model, the Au NW shows a rhombic cross-section and a round-end. Figures 3B and 3C show how the contact force of NW changes with the vertical displacement. Owing to the Euler buckling instability, with increasing vertical displacement, the contact force sharply increases and then becomes plateau.

Once the calculated relation between the vertical displacement of NW and the contact force is combined with the experimentally measured electrical resistance from buckled Au NW in Figure 2D, the relation between the contact resistance and contact force is given. As shown in Figure 3D, the contact resistance decreases with increasing compressive force, as expected as the contact area increases. When nonlinear regression was applied to the data points, the exponent in Equation 4 was initially 1.17, which corresponds to the Sharvin resistance for the plastic deformation of the contact. Furthermore, for a given applied initial load range, the contact radius can be estimated to be approximately 2 nm, which is smaller than the mean free path for Au which is approximately 8–13 nm (Jankowski and Tsakalakos, 2000). Thus, the initial contact exhibits Sharvin resistance. In contrast, the rate of resistance change decreases to a smaller extent with increasing applied load, so the

exponent decreases to 0.54, representing the Holm contact regime (Figure 3D). Compared to the previous studies (Erts et al., 2000; Useinov et al., 2020), the transition from the Sharvin to the Holm regime in this study is more abrupt owing to the limited datapoints. Nevertheless, the data points show a clear enough trend to distinguish the contact regime and determine the transition. The change in the resistance regime can also be confirmed by the I-V curves in Figure 2C. The I-V curves for the Sharvin resistance regime (for vertical displacements of 100 and 200 nm for the nanowire probe) exhibit nonlinear behavior in contrast to those for the Holm resistance regime. The nonlinear behavior of small electrical contacts is a characteristic of small quantum-transport contacts (Hibbitt, 1984; Underwood and Mulvaney, 1994). Electrical current does not uniformly flow through metal-to-metal contacts but concentrates at many tiny spots where the two metals intimately contact. It has previously been reported that for initial tiny contacts, so-called "quantum-point contacts," these tiny spots thicken with increasing electrical current, which results in a nonlinear I-V curve for the nanowire. Once the nanowire finally reaches the critical buckling load of 0.04 μN, the change of the Holm resistance is negligible, as shown in Figure 3D, because the buckling of Au nanowire results in low constant stress under 10 MPa during electrical measurements as shown in Figures 1D and 1F (stress was calculated by dividing the compression load by the area of Au NW). Notably, according to Equation 1, as the length of NW increases or the diameter of NW decreases, the critical buckling load decreases, meaning that the NW is less likely to damage the contact material. Especially, the Au NWs with thinner cross-section may show more stable and reversible buckling deformation compared to that with thicker cross-section owing to the size effect on the yield strength (Figure S3) (Seo et al., 2013). However, it should be considered that the longer or thinner the NW is, the more difficult it is to control the NW as a probe. Therefore, for practical usage, the geometry of NW should further be optimized. In this study, it is confirmed that the mechanically unstable buckling deformation of NW can be utilized to reliably measure the resistance without having to worry about variations in the contact force of the probe and sample damage.

Electrical measurement utilizing Au nanowire with Euler buckling instability

Now, we demonstrate that the stable electrical measurement at nanoscale is achievable by utilizing the Au NW that shows Euler buckling instability. Figure 4A shows a representative nanoscale electrical measurement of a silver flake using the conventional tungsten tip as a reference. We applied voltage to measure the resistance of silver flake. The corresponding V-I curve in Figure 4B shows that the voltage linearly increases with the current but also shows noticeable noises and slope changes. The noise may decrease by increasing the contact area between the tungsten tip and the silver flake. However, it leaves damages in the silver flake (Figure 4C). Figure 4D shows severe damage of the tungsten tip that may occur while trying to secure sufficient contact area by applying excessive force. The excessive force may damage the tungsten probe as well as the specimen (even fractured). On the other hand, the electrical measurement using Au NW leaves no damage to the sample and the NW, ensuring accurate and stable measurement. This is because in the buckled NW the contact stress is constant to below 10 MPa with increasing contact area. Figure 4E shows that the buckled Au NW is pinned to the silver flake. Accordingly, the corresponding V-I curve in Figure 4F shows clear linearity without any noticeable noise. This implies that we can take advantage of the mechanically unstable buckling deformation of the Au NW to reliably measure the resistance without having to worry about variations in the contact force of the probe and sample damage. For the practical resistance measurement, the Au NWs can be utilized as a probe for the four-point method on nanoscale (Considering a Joule heating leading to melting of Au NW, the maximum voltage that can be applied is 1 V). The low contact resistance originating from the Holm contact regime and the low force exerted on the specimen from the buckled Au nanowire enables reliable nanoscale electrical measurements.

The stable electrical measurement resulting from the buckling instability of NWs suggests that the findings of this study can be extended to other NWs such as Ag, Pt, Si, and ZnO as well, while the Au NW has advantages of high electrical conductivity, defect-free microstructure, corrosion/oxidation resistance, and biocompatibility. To further increase the applicability to various engineering fields, time- and cost-consuming steps in fabrication such as metal deposition and ion beam milling in this study, can be replaced by adopting a direct growth of NWs on the nano-manipulator or a force-sensing cantilever (Kang et al., 2015; Yoo et al., 2010).

In conclusion, we systematically quantified the buckling behavior of Au NW and characterized their contact resistance under compressive loading. Our dislocation-free, single-crystalline Au nanowire did not fail, and showed classical Euler buckling with extremely reversible. During compressive deformation in the Au nanowire probe, the contact area increased with increasing load, resulting in a decrease in contact resistance. The electron transport at contacts initially was quantum transport exhibiting Sharvin contact resistance. As an increasing amount of load was applied to the probe tip, classical diffusive transport dominated because

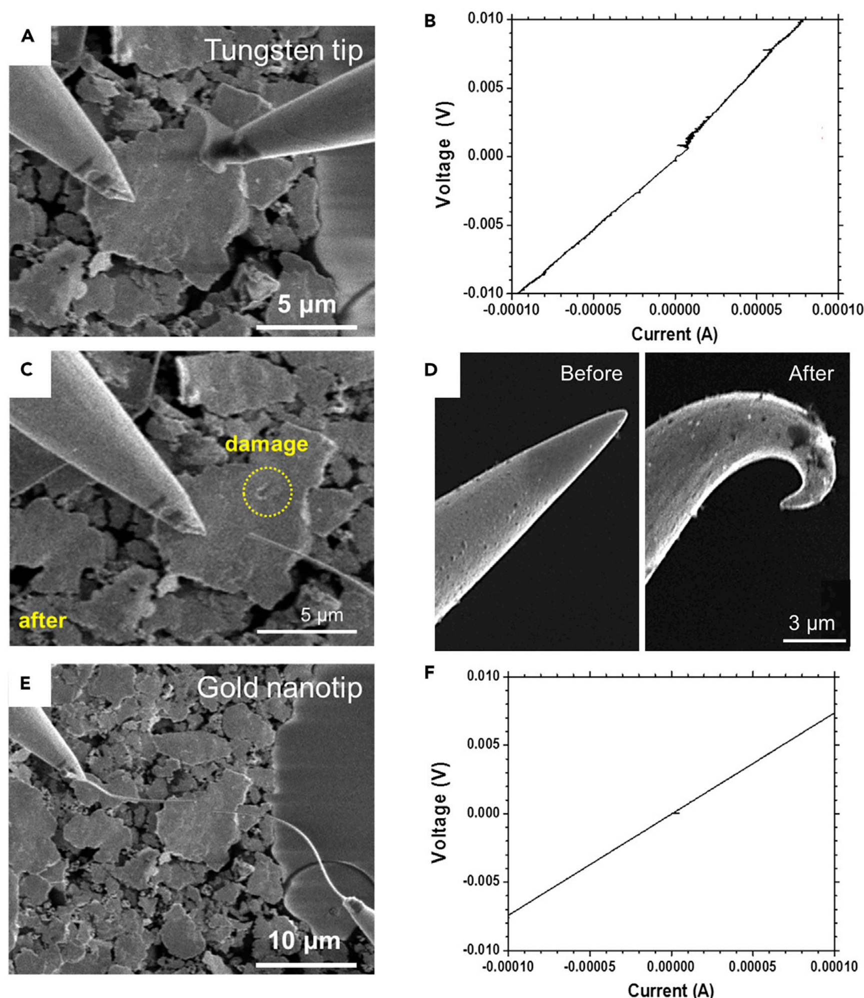

Figure 4. Electrical measurement utilizing conventional tungsten tip (A–D) and Au nanowire (E and F) with Euler buckling instability

(A) SEM image of silver flake and conventional tungsten tip for the electrical measurement.
(B) I-V curves measured by tungsten tip.
(C) SEM image of silver flake after the measurement.
(D) SEM image of tungsten tip before and after the electrical measurement.
(E) SEM image of silver flake and Au nanowire for the electrical measurement.
(F) I-V curves measured by Au nanowire.

the Holm contact has the lowest resistance. After a minimum amount of load was applied to the probe tip, buckling-assisted deformation enabled a stable contact area to be maintained because of the constant buckling load. The Sharvin to Holm transport phenomena owing to the buckling of the conductive Au nanowire SPM probe enables electrical properties to be reliably measured at the nanoscale.

Limitations of the study

This study demonstrates the potential of Au nanowires as stable electrical probes. To increase the applicability, the fabrication process and the geometry of nanowires need to be further optimized.

STAR★METHODS

Detailed methods are provided in the online version of this paper and include the following:

- KEY RESOURCES TABLE
- RESOURCE AVAILABILITY

- Lead contact
- Materials availability
- Data and code availability
- METHOD DETAILS
  - Cyclic buckling test of Au nanowire probe
  - The electrical measurement process of Au nanowire probe
  - FE analysis

SUPPLEMENTAL INFORMATION

Supplemental information can be found online at https://doi.org/10.1016/j.isci.2022.105199.

ACKNOWLEDGMENTS

This research was funded by the National Research Foundation of Korea (NRF) (No. NRF-2020R1A5A6017701 and 2019R1A2C2003430) and supported by the Creative-Pioneering Researchers Program through Seoul National University.

AUTHOR CONTRIBUTIONS

J.H.S. and J.P.A. conceived and designed the experiments. S.G.K., Y.C., H.S.P., and I.S.C. conducted the computational analysis. Y.Y. and B.S.K. fabricated Au nanowires. All authors analyzed and discussed the results. J.P.A. B.S.K. and I.S.C. supervised the project.

DECLARATION OF INTERESTS

The authors declare no competing interests.

Received: May 9, 2022
Revised: August 29, 2022
Accepted: September 20, 2022
Published: October 21, 2022

REFERENCES

Avramov, K.V., and Mikhlin, Y.V. (2016). Snap-through truss as a vibration absorber. J. Vib. Control *10*, 291–308. https://doi.org/10.1177/1077546304035604.

Begley, M.R., and Barker, N.S. (2007). Analysis and design of kinked (bent) beam sensors. J. Micromech. Microeng. *17*, 350–357. https://doi.org/10.1088/0960-1317/17/2/022.

Cottone, F., Gammaitoni, L., Vocca, H., Ferrari, M., and Ferrari, V. (2012). Piezoelectric buckled beams for random vibration energy harvesting. Smart Mater. Struct. *21*, 035021. https://doi.org/10.1088/0964-1726/21/3/035021.

Dobrokhotov, V.V., Yazdanpanah, M.M., Pabba, S., Safir, A., and Cohn, R.W. (2008). Visual force sensing with flexible nanowire buckling springs. Nanotechnology *19*, 035502. https://doi.org/10.1088/0957-4484/19/03/035502.

Elvin, N.G., Lajnef, N., and Elvin, A.A. (2006). Feasibility of structural monitoring with vibration powered sensors. Smart Mater. Struct. *15*, 977–986. https://doi.org/10.1088/0964-1726/15/4/011.

Erbil, S.O., Hatipoglu, U., Yanik, C., Ghavami, M., Ari, A.B., Yuksel, M., and Hanay, M.S. (2020). Full electrostatic control of nanomechanical buckling. Phys. Rev. Lett. *124*, 046101. https://doi.org/10.1103/PhysRevLett.124.046101.

Erts, D., Olin, H., Ryen, L., Olsson, E., and Thölén, A. (2000). Maxwell and Sharvin conductance in gold point contacts investigated using TEM-STM. Phys. Rev. B *61*, 12725–12727. https://doi.org/10.1103/PhysRevB.61.12725.

Hibbitt, H.D. (1984). ABAQUS/EPGEN—a general purpose finite element code with emphasis on nonlinear applications. Nucl. Eng. Des. *77*, 271–297.

Holm, R. (1967). Electrical Contacts: Theory and Application (Springer-Verlag).

Hsin, C.-L., Mai, W., Gu, Y., Gao, Y., Huang, C.-T., Liu, Y., Chen, L.-J., and Wang, Z.-L. (2008). Elastic properties and buckling of silicon nanowires. Adv. Mater. *20*, 3919–3923. https://doi.org/10.1002/adma.200800485.

Hwang, B., Kang, M., Lee, S., Weinberger, C.R., Loya, P., Lou, J., Oh, S.H., Kim, B., and Han, S.M. (2015). Effect of surface energy on size-dependent deformation twinning of defect-free Au nanowires. Nanoscale *7*, 15657–15664. https://doi.org/10.1039/c5nr03902a.

Jankowski, A.F., and Tsakalakos, T. (2000). The effect of strain on the elastic constants of noble metals. J. Phys. F Met. Phys. *15*, 1279–1292.

Ji, L.-W., Young, S.-J., Fang, T.-H., and Liu, C.-H. (2007). Buckling characterization of vertical ZnO nanowires using nanoindentation. Appl. Phys. Lett. *90*, 033109. https://doi.org/10.1063/1.2431785.

Kang, M., Lee, H., Kang, T., and Kim, B. (2015). Synthesis, properties, and biological application of perfect crystal gold nanowires: a review. J. Mater. Sci. Technol. *31*, 573–580. https://doi.org/10.1016/j.jmst.2015.01.007.

Kiyono, C.Y., Silva, E.C.N., and Reddy, J.N. (2012). Design of laminated piezocomposite shell transducers with arbitrary fiber orientation using topology optimization approach. Int. J. Numer. Methods Eng. *90*, 1452–1484. https://doi.org/10.1002/nme.3371.

Kleinbichler, A., Pfeifenberger, M.J., Zechner, J., Wöhlert, S., and Cordill, M.J. (2018). Scratch induced thin film buckling for quantitative adhesion measurements. Mater. Des. *155*, 203–211. https://doi.org/10.1016/j.matdes.2018.05.062.

Mikrajuddin, A., Shi, F.G., Kim, H.K., and Okuyama, K. (1999). Size-dependent electrical constriction resistance for contacts of arbitrary size: from Sharvin to Holm limits. Mater. Sci. Semicond. Process. *2*, 321–327.

Ramlan, R., Brennan, M.J., Mace, B.R., and Burrow, S.G. (2012). On the performance of a dual-mode non-linear vibration energy harvesting device. J. Intell. Mater. Syst. Struct. *23*,

CellPress
OPEN ACCESS

1423–1432. https://doi.org/10.1177/1045389x12443017.

Seo, J.H., Park, H.S., Yoo, Y., Seong, T.Y., Li, J., Ahn, J.P., Kim, B., and Choi, I.S. (2013). Origin of size dependency in coherent-twin-propagation-mediated tensile deformation of noble metal nanowires. Nano Lett. *13*, 5112–5116. https://doi.org/10.1021/nl402282n.

Seo, J.H., Yoo, Y., Park, N.Y., Yoon, S.W., Lee, H., Han, S., Lee, S.W., Seong, T.Y., Lee, S.C., Lee, K.B., et al. (2011). Superplastic deformation of defect-free Au nanowires via coherent twin propagation. Nano Lett. *11*, 3499–3502. https://doi.org/10.1021/nl2022306.

Sharvin, Y.V. (1965). On the possible method for studying fermi surfaces. Sov. Phys. JETP *21*, 655–656.

Shaw, A.D., Neild, S.A., Wagg, D.J., Weaver, P.M., and Carrella, A. (2013). A nonlinear spring mechanism incorporating a bistable composite plate for vibration isolation. J. Sound Vib. *332*, 6265–6275. https://doi.org/10.1016/j.jsv.2013.07.016.

Song, J., Jiang, H., Choi, W.M., Khang, D.Y., Huang, Y., and Rogers, J.A. (2008a). An analytical study of two-dimensional buckling of thin films on compliant substrates. J. Appl. Phys. *103*, 014303. https://doi.org/10.1063/1.2828050.

Song, J., Jiang, H., Liu, Z.J., Khang, D.Y., Huang, Y., Rogers, J.A., Lu, C., and Koh, C.G. (2008b). Buckling of a stiff thin film on a compliant substrate in large deformation. Int. J. Solid Struct. *45*, 3107–3121. https://doi.org/10.1016/j.ijsolstr.2008.01.023.

Sun, Y., Choi, W.M., Jiang, H., Huang, Y.Y., and Rogers, J.A. (2006). Controlled buckling of semiconductor nanoribbons for stretchable electronics. Nat. Nanotechnol. *1*, 201–207. https://doi.org/10.1038/nnano.2006.131.

Timoshenko, S.P., and Gere, J.M. (1961). Theory of Elastic Stability (McGraw-Hill).

Underwood, S., and Mulvaney, P. (1994). Effect of the solution refractive index on the color of gold colloids. Langmuir *10*, 3427–3430. https://doi.org/10.1021/la00022a011.

Useinov, A., Lin, H.H., Useinov, N., and Tagirov, L. (2020). Spin-resolved electron transport in nanoscale heterojunctions. Theory and applications. J. Magn. Magn Mater. *508*, 166729. https://doi.org/10.1016/j.jmmm.2020.166729.

Van Blarigan, L., Danzl, P., and Moehlis, J. (2012). A broadband vibrational energy harvester. Appl. Phys. Lett. *100*, 253904. https://doi.org/10.1063/1.4729875.

Vandamme, L.K.J. (1974). 1/f noise of point contacts affected by uniform films. J. Appl. Phys. *45*, 4563–4565. https://doi.org/10.1063/1.1663088.

Wang, G.-F., and Feng, X.-Q. (2009). Surface effects on buckling of nanowires under uniaxial compression. Appl. Phys. Lett. *94*, 141913. https://doi.org/10.1063/1.3117505.

Yang, Y., Tang, L., and Li, H. (2009). Vibration energy harvesting using macro-fiber composites. Smart Mater. Struct. *18*, 115025. https://doi.org/10.1088/0964-1726/18/11/115025.

Yoo, Y., Seo, K., Han, S., Varadwaj, K.S.K., Kim, H.Y., Ryu, J.H., Lee, H.M., Ahn, J.P., Ihee, H., and Kim, B. (2010). Steering epitaxial alignment of Au, Pd, and AuPd nanowire arrays by atom flux change. Nano Lett. *10*, 432–438. https://doi.org/10.1021/nl903002x.

Zhou, H., Qin, W., Yu, Q., Chen, F., Yu, X., Cheng, H., and Wu, H. (2019). Controlled buckling and postbuckling behaviors of thin film devices suspended on an elastomeric substrate with trapezoidal surface relief structures. Int. J. Solid Struct. *160*, 96–102. https://doi.org/10.1016/j.ijsolstr.2018.10.018.

Zhu, Y., and Zu, J.W. (2013). Enhanced buckled-beam piezoelectric energy harvesting using midpoint magnetic force. Appl. Phys. Lett. *103*, 041905. https://doi.org/10.1063/1.4816518.

STAR★METHODS

KEY RESOURCES TABLE

REAGENT or RESOURCE	SOURCE	IDENTIFIER
Others		
Quanta FEI DualBeam^{TM} microscope	FEI	https://www.labwrench.com/equipment/7341/fei-company-quanta-trade-3d-dualbeam-trade
Nanomanipulator MM3A	Kleindieck	https://www.nanotechnik.com/mm3a-em.html
Force measurement FMS-EM	Sigma-Aldrich	https://www.nanotechnik.com/fms-em.html
Electrical measurement B1500	Keysight	https://www.keysight.com/de/de/products/parameter-device-analyzers-curve-tracer/precision-current-voltage-analyzers/b1500a-semiconductor-device-parameter-analyzer.html
Software and algorithms		
Abaqus Standard Ver. 6.10	Simulia	https://www.3ds.com/products-services/simulia/products/abaqus/
Origin 2019	OriginLab	https://www.originlab.com/2019

RESOURCE AVAILABILITY

Lead contact

Further information and requests for resources and reagents should be directed to and will be fulfilled by the lead contact, Prof. In-Suk Choi (insukchoi@snu.ac.kr).

Materials availability

This study did not generate new unique reagents.

Data and code availability

Data reported in this paper will be shared by the lead contact upon request. This paper does not report original code. Any additional information required to reanalyze the data reported in this paper is available from the lead contact upon request.

METHOD DETAILS

Cyclic buckling test of Au nanowire probe

The various buckling behavior modes of the nanowires were investigated by compressing free-standing Au nanowire (Mov. S1) and Au nanowires fixed at both ends (Mov. S2) at a compression rate of 1.9×10^{-7} m/s. The buckling load of the nanowires that had both ends fixed was measured using the Si-cantilever-based force measurement system (FMS-EM, Kleindiek). One end of an Au nanowire was first attached to a commercial tungsten probe for the nanomanipulator (MM3A, Kleindeck), and e-beam assisted Pt deposition was then used to weld the other end of the Au nanowire onto the Si cantilever. The ends of the Au nanowire were subsequently compressed at a rate of 1.9×10^{-7} m/s.

The electrical measurement process of Au nanowire probe

To investigate the electrical contact resistance of the Au nanowires during buckling, we contacted the Au nanowire to the surface of a bulk Au electrode and subsequently measured I-V curves during buckling (B1500, Agilent and STA, Keysight). All experiments were conducted using the FEI DualBeam^{TM} microscope.

FE analysis

We conducted FE analysis on the Euler buckling deformation of Au nanowire using general FE analysis software (ABAQUS/Standard (Ver. 6.10), Dassault Systèmes, Vélizy-Villacoublay, France). The deformation of the Au nanowire was assumed to be linearly elastic. We established a 3D model based on the actual geometry with adaptive meshing.